Hydrodynamic Characteristics of an Electric Eel-Like Undulating Fin

M. Zhang [1, 2†], C. Wang [1] and Y. Su [1]

[1] *Shandong University of Science and Technology, Qingdao, 266590, China*
[2] *Anhui Province Key Laboratory of Special Heavy Load Robot, Maanshan, 243032, China*

†*Corresponding Author Email: m.h.zhang@sdust.edu.cn*

ABSTRACT

Taking the electric eel as a bionic object, a long undulatory fin is designed. The turbulent model standard k-ε is used to solve the N–S equation of a three-dimensional unsteady incompressible fluid. The hydrodynamic characteristics of the undulatory fin are studied, and the influence of the swing angle, wave frequency and ground effects on the propulsion performance of the undulatory fin are discussed. The mathematical models of the average thrust and average lateral force of the undulatory fin are established by using multiple linear regression. The results show that the thrust and lateral force of the undulatory fin increase with increasing swing angle and swing frequency, but in a motion period, the number of fluctuations of the thrust is approximately twice that of the lateral force. The relationship between the average thrust force and the average lateral force of the undulatory fin and the wave frequency and the maximum swing angle satisfies a specific exponential law. When the undulating fin moves near the wall ($d \leq 0.2\ W$), due to the coupling between the vortex at the lower edge and the tail vortex where part of the vortex is transferred to the two sides, the total thrust decreases, and the lateral force increases.

NOMENCLATURE

l	length along x-axis	x_i, x_j	Cartesian coordinates
s	length along the fin	u_i, u_j	velocity in i and j directions
f	swing frequency of the fin	k	turbulent kinetic energy
T	swing period of the fin	ε	turbulent dissipation
t	time	μ_t	turbulent viscosity coefficient
F_{tm}	average thrust force (along x direction)	S_k	customized turbulent kinetic energy term
F_{lm}	average lateral force (along z direction)	S_ε	turbulent dissipation term
$F_t(t)$	thrust force acting on undulatory fin	Y_M	contribution term of turbulence fluctuation to dissipation rate
$F_l(t)$	lateral force acting on undulatory fin	G_b	turbulent kinetic energy term generated by buoyancy
A	area undulatory fin		
p	pressure acting on undulatory fin	G_k	turbulent kinetic energy term generated by velocity gradient
λ	wave length generated by the fluctuating fin		
ρ	fluid density	Ω	rotary rate tensor
μ	fluid dynamic viscosity	S	deformation rate tensor
α_{max}	maximum swing angle of the fin swinging to one side		

1. INTRODUCTION

Propulsion technology is the key technology for high-performance underwater vehicles. Currently, three prevailing underwater propulsion methods include propeller propulsion, water jet propulsion and bionic propeller propulsion which replicates the characteristics of natural biological movement (Liu 2015). An ideal underwater vehicle should operate

efficiently in an unsteady flow with variable depth and frequent changes in speed. The first two methods have some intrinsic defects: the propeller is easily entangled by water weeds and does not have manoeuvrability at low speed or when hovering, and its propulsion efficiency is low in unsteady flow (Suzuki and Kato 2005). Water jet propulsion is only suitable for shallow water navigation (Deng 2015). Due to their evolution, fish can manoeuvre efficiently in variable water environments by adjusting their swimming manner correspondingly. The median and/or paired fin (MPF) propulsion mode has good manoeuvrability and propulsion efficiency in the low-speed swimming state (Kato 2005). Researchers have conducted much research on a propulsion mode that imitates the MPF of fish, especially in the design of undulatory fins. Xiao *et al.* (2021) designed an amphibious robot based on the motion mode of the electric eel. Ma *et al.* (2019) designed three fin surface waveforms and found that when the distance is close to the wall, the fin produces nearly zero thrust and the largest lateral force. Yin *et al.* (2021) designed an undulatory fin that exerted preload on the fin surface to produce deformation and found that when the flow is turbulent, the tangential force can be neglected. Nguyen *et al.* (2018) designed a modular undulatory fin using the Grooved Cam System, and the thrust is maximum when the frequency is 3 Hz. Arslan and Kadir (2019) designed the propulsion system of an amphibious robot by using a crank rocker mechanism to simulate the sine wave motion of squid fins. Liu *et al.* (2020) proposed a hybrid structure control system with the phase control method to optimize propulsion system of undulating fin. Zhang *et al.* (2021) designed an underwater vehicle with hybrid propulsion and adopt central pattern generators model and fuzzy adaptive proportion integral differential to keep low-speed stability and maneuverability. Wang *et al.* (2015) design a new robotic fish inspired by the freshwater stingray and the heave force reaches its minimum when the wave number is at 1. Zhao and Dou (2019) discussed the impact of the phase-angle and the angular amplitude

on the thrust and heave forces. He *et al.* (2015) built an underwater vehicle using shape memory alloy fins which performances depend on the arrangements of multiple fins and the gap between the fins. Wang *et al.* (2019) designed a robotic fish having optimal wave efficiency and locomotor performance when the Strouhal number is at the range of 0.2–0.4. Li *et al.* (2021) analysed the vortex structure and its relationship with thrust, heave force using diffusion-based smoothing model and PIV experiments.

In addition, there are also many studies on the influence of motion parameters on the hydrodynamic characteristics of undulatory fins. Liu and Curet (2018) use particle image velocimetry to measure swimming speed and direction angle around the undulatory fin in order to understand its maneuverability and performance. Zhang *et al.* (2019) found that there are manifold

vortices, crescent vortices and annular vortices around the fluctuating fin and described the characteristics of the vortices. Wei *et al.* (2021) analysed the change in the propulsion efficiency of fish-like propulsion with wavelength and frequency. Moored (2018) calculate hydrodynamic characteristics of the undulating fin adopt an unsteady three-dimensional boundary element method. Sun *et al.* (2019) perform comprehensive parametric study of an undulating plate which has a high-efficiency area when the wave speed is at 0.6 and the wavelength is approximately 0.3 times the fin length. Luo *et al.* (2020) discuss the propulsive performance of caudal fin model with different stiffness distributions. For the multiundulatory fin propeller, the effects of the phase difference, wavenumber and aspect ratio of the front and rear fins on the propulsion performance are also studied (Shi *et al.* 2021a; Pang *et al.* 2021; Yin *et al.* 2021). Moreover, the ground effect on the lift and thrust forces has been studied (Zhang *et al.* 2017; Park *et al.* 2017; Mivehchi *et al.* 2016; Shi *et al.* 2021b).

In summary, previous research has mainly focused on the two-dimensional numerical simulation of undulating fins. Although two-dimensional numerical simulation can obtain the hydrodynamic characteristics and wake vortex distribution of undulating fins, it cannot show the distribution of velocity, pressure and lateral vortex along the width direction. Moreover, in the design of undulatory fins, the structural parameters mostly come from experimental data (Mohamad *et al.* 2022; Lawag and Ali 2022). To fill these gaps, the work of this paper is as follows: (1) Taking the electric eel as the bionic object, an undulatory long fin propeller driven by a single motor is designed. The effects of the fin swing angle, wave frequency and wall effect of the three-dimensional undulatory fin on the propulsion performance are studied. (2) the multilinear mathematical regression model is established, considering the parameters that affect the hydrodynamic characteristics: wave frequency and maximum swing angle.

The paper is organized as follows: The kinematic model of the undulatory fin is set up and the turbulent model of the numerical simulation is discribed in the second section. In the third section, the numerical simulation results, the theoretical calculation using the multilinear mathematical regression model are obtained. Finally, the findings and conclusion of the present study are given.

2. PROBLEM DESCRIPTION AND NUMERICAL METHODS

2.1 Structure and Kinematics Model of Undulating Fin

In this paper, taking the electric eel as the bionic object, an undulatory fin that drives the flexible fin surface to realize approximate sinusoidal vibration is designed. The the fin of an electric eel, driving mechanism and fin surface shape of the undulatory fin are shown in Fig. 1. The length of the
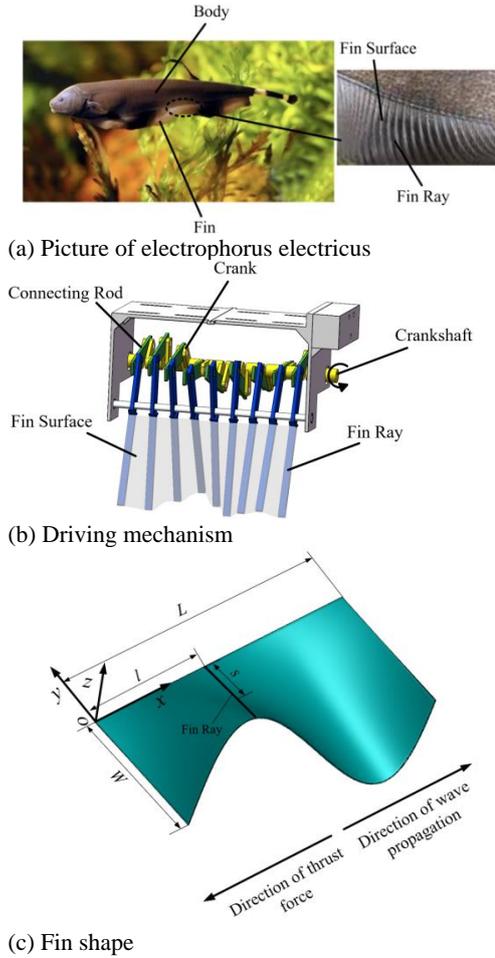
(a) Picture of electrophorus electricus

(b) Driving mechanism

(c) Fin shape

Fig. 1. Structure diagram of the undulating fin.

undulatory fin is L=240 mm, and the width is W=140 mm.

The coordinate system is defined by x, y and z, which represent the moving direction, vertical direction and swinging direction of the fin, respectively. The wave equation of the fin surface is as follows:

$$
\begin{cases}
x(l,s,t)=l \\
y(l,s,t)=s \cdot \cos(\alpha)=s \cdot \cos\left\{\alpha_{\max}\sin\left[2\pi\left(f\cdot t-\dfrac{l}{\lambda}\right)\right]\right\} \\
z(l,s,t)=s \cdot \sin(\alpha)=s \cdot \sin\left\{\alpha_{\max}\sin\left[2\pi\left(f\cdot t-\dfrac{l}{\lambda}\right)\right]\right\}
\end{cases}
$$
(1)

The swing angle of the ith fin with time t is defined as follows:

$$
\alpha_i(l_i,t)=\alpha_{\max}\sin\left[2\pi\left(f\cdot t-\frac{l_i}{\lambda}\right)\right] \quad i=1,\ 2\ldots9 \quad (2)
$$

Since the undulating fin fluctuates periodically, the force acting on the surrounding fluid changes periodically with time. The average thrust force (along the x-direction) and the average lateral force (along the z-direction) are calculated using the time average method, which are written as follows:

$$
F_{tm}=\frac{1}{T}\int_T F_t(t)\,\mathrm{d}t=\frac{1}{T}\int_T\int_S p\left(n_x\cdot\mathrm{d}A\right)\,\mathrm{d}t
$$
(3)

$$
F_{lm}=\frac{1}{T}\int_T F_l(t)\,\mathrm{d}t=\frac{1}{T}\int_T\int_S p\left(n_z\cdot\mathrm{d}A\right)\,\mathrm{d}t
$$
(4)

2.2 Turbulence Model

The tuebulence model k-ε is adopted to simulate the hydrodynamic characteristics of the undulatory fin, and its transport equation is as follows (Hussain *et al.* 2022; Alqahtani *et al.* 2023):

$$
\frac{\partial(\rho k)}{\partial t}+\frac{\partial(\rho k u_i)}{\partial x_i}=\frac{\partial}{\partial x_j}\left[\left(\mu+\frac{\mu_t}{\sigma_k}\right)\frac{\partial k}{\partial x_j}\right]+
$$
$$
G_k+G_b-\rho\varepsilon-Y_M+S_k
$$
(5)

$$
\frac{\partial(\rho\varepsilon)}{\partial t}+\frac{\partial(\rho\varepsilon u_i)}{\partial x_i}=\frac{\partial}{\partial x_j}\left[\left(\mu+\frac{\mu_t}{\sigma_\varepsilon}\right)\frac{\partial\varepsilon}{\partial x_j}\right]+
$$
$$
C_{1\varepsilon}\frac{\varepsilon}{k}\left(G_k+C_{3\varepsilon}G_b\right)-C_{2\varepsilon}\rho\frac{\varepsilon^2}{k}+S_\varepsilon
$$
(6)

where

$\sigma_k=1.0$, $\sigma_\varepsilon=1.0$, $C_{1\varepsilon}=1.44$, $C_{2\varepsilon}=1.92$, and $C_{3\varepsilon}=0.09$ (Zawawi *et al.* 2022).

2.3 Mesh Generation and Boundary Conditions

The calculation domain of the undulatory fin model is shown in Fig. 2. The original point is located at the apex of the front end of the fin surface. The external flow field is a 1920 mm × 960 mm × 600 mm cuboid. The distance from the front end of the undulatory fin to the inlet boundary is 480 mm, and the distance from the trailing edge to the outlet boundary is 1200 mm. The boundary conditions are set as velocity inlet, pressure outlet, and other boundaries are nonslip walls. The boundary parameters are shown in Table 1. Please note that the inlet velocity in Table 1 is not close to the specific velocity of an electric eel, which is upstream flow velocity when undulating fin undulates. The inlet velocity of 0.01m/s can be approximately regarded as undulating fins in static water. Therefore, the thrust and lateral force generated by the undulating fin's own fluctuation can be obtained and the flow resistance can be ignored. The FLUENT software is adopted to simulate the flow field.

Table 1 Boundary condition setting

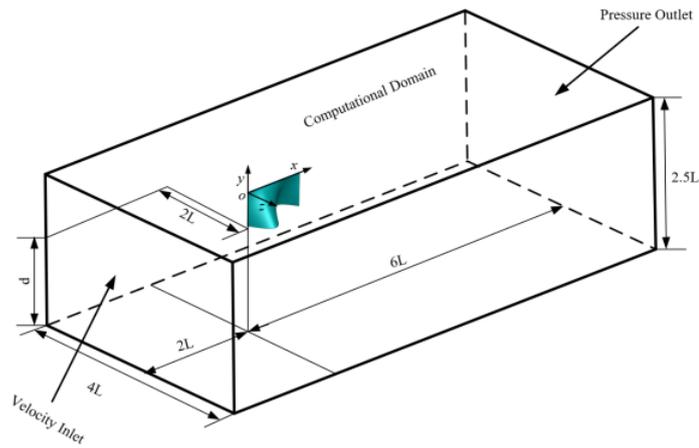| The boundary of computational domain	Boundary condition setting
Inlet	U_0=0.01 m/s
Outlet	p_{out}=0
The others boundary	wall

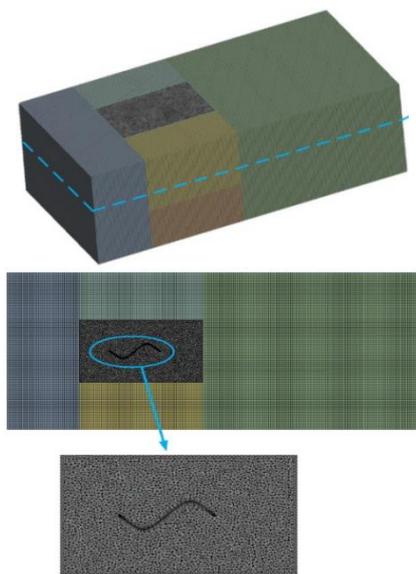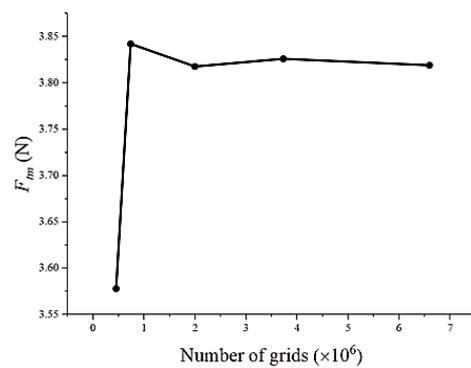**Fig. 2. Calculation area model diagram of the undulating fin.**

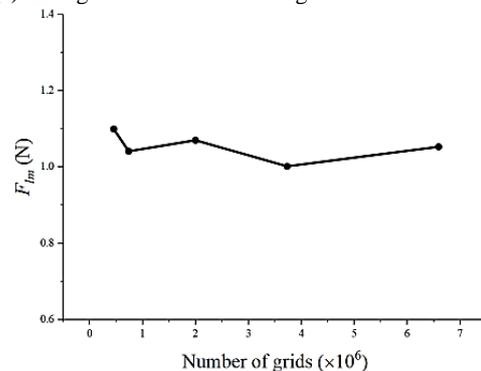**Fig. 3. Mesh model of the undulating fin.**

Due to the complex shape of the undulatory fin, a structural mesh is used in the external flow field, and a dynamic unstructured mesh is used around the undulatory fin. The Define_Grid_Motion macro is adopted to control its boundary motion according to the fluctuation law of fin surface. The mesh model is shown in Fig. 3.

2.4 Mesh Independence Verification

The number of grids affects the accuracy of the calculation results, convergence and calculation time. To verify mesh independence, five grid numbers (0.45×10^6 , 0.73×10^6 , 1.99×10^6 , 3.73×10^6 , 6.59×10^6) are adopted to calculate the performance of the undulatory fin. The frequency is set to f = 2.5 Hz, the maximum swing angle is set to α_{max}=30° , and the wavenumber is set to λ=1 . The distance between the end of the undulatory fin and the bottom is d=2.5 W, and the inflow velocity is 0.01 m/s. The time step size is set to 10^{-3} s. The changes in thrust force and lateral force with the grid numbers is shown in Fig. 4. When the number

(a) Change in thrust force with grid number

(b) Change in lateral force with grid number
Fig. 4. Change of force with grid number.

of grids reaches 1.99×10^6, the results are basically stable. Therefore, the grid number 1.99×10^6 was used for numerical simulation.

2.5 Validation of the Turbulence Model and Numerical Method

To validate the turbulence model and numerical method, we calculated the fin discussed by Zhou *et al.* (2010) at the same working conditions. The wave number is 1, the swing frequency is 2.0 Hz, and the undulating amplitude is 0.02 m. As shown in Fig. 5, the present simulation results of the thrust force with different inlet velocities are identical with those given by Zhou *et al.* (2010).
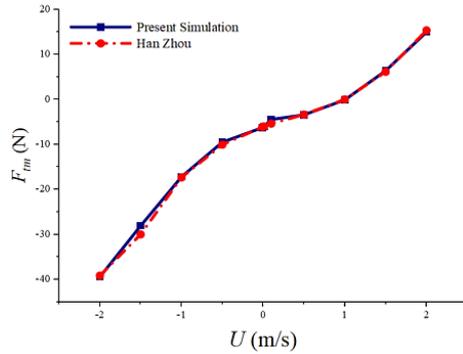
Fig. 5. Change of average thrust force with inlet velocity.

3. NUMERICAL SIMULATION RESULTS AND DISCUSSION

3.1 Study on the Hydrodynamic Characteristics of an Undulatory Fin

To study the hydrodynamic characteristics and explore the thrust source of the undulatory fin, the undulatory fin with a maximum swing angle of $a_{max}=30°$ and a swing frequency of $f = 2.5$ Hz was selected. Figure 6 shows the change in the surface pressure of the undulatory fin in a fluctuation period. The high-pressure area always appears at the front edge of the concave surface of the undulatory fin, and its corresponding convex position is the low-pressure area. That is, fin surface fluctuation makes the surrounding fluid form a pressure difference on both sides in the same direction as the moving direction of the undulatory fin, which is an important source of the thrust force. The high-pressure region moves from the front end to the trailing edge along the propagation direction of the travelling wave with the fluctuation of the fin. The alternation of high and low pressure makes the force acting on the undulatory fin fluctuate sinusoidally.

The change in the velocity vector in a fluctuation period is shown in Fig. 7. The velocity of the fluid around the undulatory fin is significantly accelerated as the fin surface fluctuates. The fluid velocity near the concave surface is greater than that near the convex surface. Because the travelling wave generated by the undulating fin always propagates from the leading edge of the fin surface to the rear-end, the fin continuously compresses the surrounding fluid during propagation, which increases the fluid velocity in the concave region. When the fin surface fluctuates, the fluid gradually flows from the front edge of the undulatory fin to the rear edge along the fin surface and finally forms a jet at the tail of the undulatory fin, which also provides thrust force for the undulatory fin.

In addition, the vorticity field around the undulatory fin is also studied. Compared with other methods, the Q criterion requires less computation when extracting vorticity, so we use the Q criterion to identify the vorticity around the undulatory fin. The calculation method of the Q criterion is shown in Eq. 7.

$$Q = \frac{1}{2}\left(\left\|\Omega^2\right\| - \left\|S^2\right\|\right) = -\frac{1}{2}\left(\left(\frac{\partial u}{\partial x}\right)^2 + \left(\frac{\partial v}{\partial y}\right)^2 + \left(\frac{\partial w}{\partial z}\right)^2\right) - \frac{\partial u}{\partial y}\frac{\partial v}{\partial x} - \frac{\partial u}{\partial z}\frac{\partial w}{\partial x} - \frac{\partial v}{\partial z}\frac{\partial w}{\partial y} \tag{7}$$

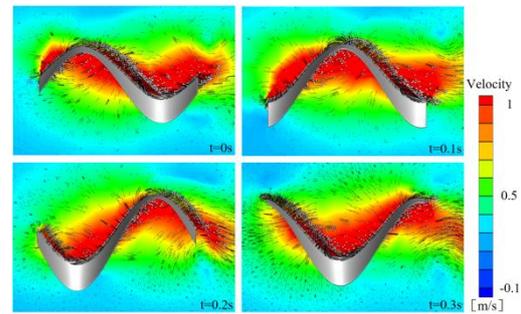Where, u, v and w are the components of wave velocity in the x, y and z directions.

Fig. 7. Variation in velocity around the undulating fin ($a_{max}=30°$, $f = 2.5$ Hz, $U_0=0.01$ m/s).
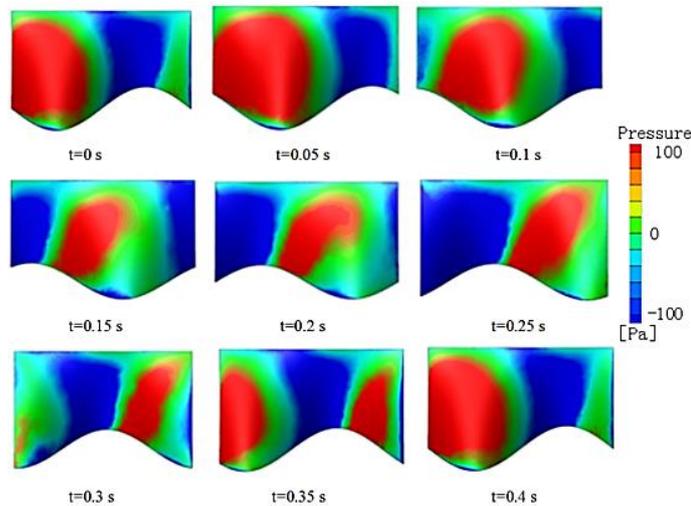

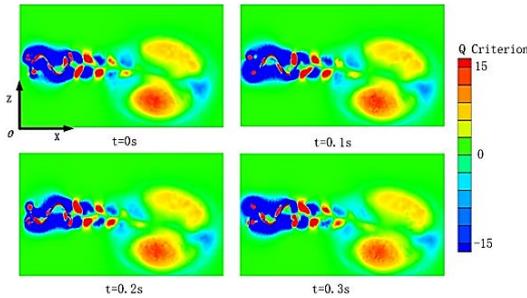**Fig. 6. Variation in pressure around the undulating fin ($a_{max}=30°$, $f = 2.5$ Hz, $U_0=0.01$ m/s)**

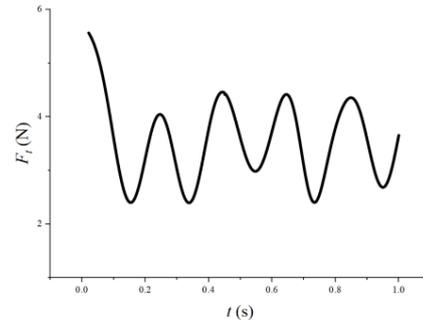**Fig. 8. Variation in vorticity around the undulating fin (a_{max}=30°, f = 2.5 Hz, U_0=0.01 m/s).**

The contour map of vorticity around the undulatory fin changing with time is shown in Fig. 8. There are always vortex rotating in opposite direction on two flanks of the fin surface. These two kinds of reverse vortices are always produced at the leading edge, gradually spread to the trailing edge, and finally fall off, which form a relatively obvious anti-Carmen vortex street.

The change in the force acting on the fin surface with time is shown in Fig. 9. The thrust force fluctuates with time, and the direction of total thrust force is the reverse of the wave propagation (shown in Fig. 9 (a)). The value of the lateral force fluctuates periodically with time near the 0 point, and the orientation of the lateral force will also alternately cycle from positive to negative (shown in Fig. 9 (b)). In addition, the number of fluctuations of thrust in a motion cycle is twice that of the lateral force. This is because during the movement of the fin, the orientation of the thrust force is always the same, but the magnitude changes, while the orientation of the lateral force will change periodically. When the value of the lateral force amount to 0, the lateral force changes direction as the undulating fin continues to move, and the inflection point appears when the reverse direction increases to the maximum value. Compared with the thrust, the lateral force increases a process of reverse pulsation.
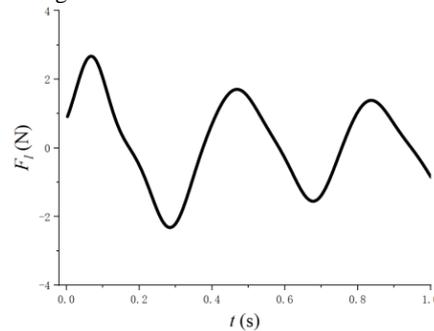
3.2 Effect of Kinematic Parameters on the Propulsion Characteristics of the Undulatory Fin

To explore the effect of kinematic parameters on the propulsion characteristics of undulatory fins, the variation law of the thrust force and lateral force are studied with different maximum swing angles of fins $\alpha_{max} = 10°, 20°, 30°$ and different wave frequencies $f = 1.0, 1.5, 2.0, 2.5, 3.0$ Hz. The average thrust and average lateral force of fluctuating fins varing with frequency in a period at different maximum fin swing angles are shown in Fig. 10 (a) and Fig. 10 (b), respectively. The average thrust and average lateral force increase with increasing maximum swing angle. In addition, the amplitude of the thrust force increasing with frequency is greater than that of the lateral force increasing with frequency. With the increase in the maximum swing angle, the curve of thrust force

changing with frequency becomes steeper. However, the variation trend of the lateral force with frequency is very close with the increase in the maximum swing angle. The average thrust force is more sensitive to changes in the swing angle than the lateral force.
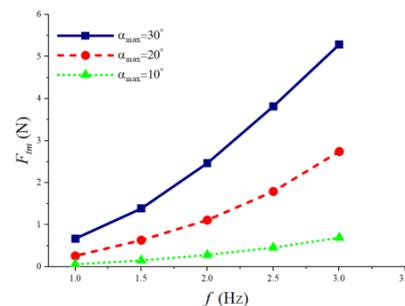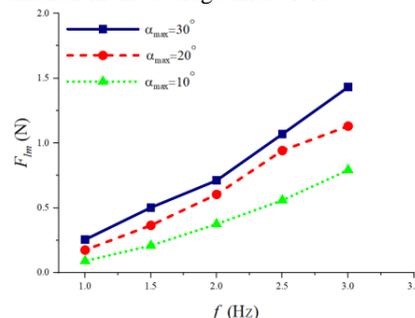

(a) Change in thrust force with time

(b) Change in lateral force with time

Fig. 9. Variation in the force acting on the undulatory fin with time (a_{max}=30°, f = 2.5 Hz, U_0=0.01 m/s).

(a) Variation in the average thrust force

(b) Variation in the average lateral force

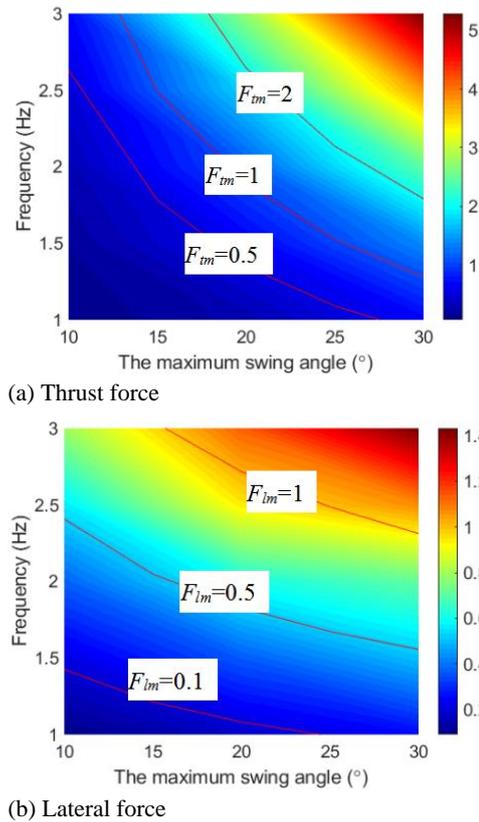**Fig. 10. The propulsive performance with frequency, U_0=0.01 m/s.**

(a) Thrust force

(b) Lateral force

Fig. 11. Force contour of the swing frequency against the maximum swing angle, U_0=0.01 m/s

Table 2 Thrust force results.

		f=1.5 Hz	f=2.5 Hz
$\alpha_{max} = 10°$	Sim.	0.2103	0.5596
	Cal.	0.2190	0.5348
$\alpha_{max} = 20°$	Sim.	0.3663	0.8931
	Cal.	0.3543	0.8652
$\alpha_{max} = 30°$	Sim.	0.4735	1.1702
	Cal.	0.4694	1.1465

Table 3 Lateral force results

		f=1.5 Hz	f=2.5 Hz
$\alpha_{max} = 10°$	Sim.	0.1534	0.4601
	Cal.	0.1566	0.4497
$\alpha_{max} = 20°$	Sim.	0.6358	1.7945
	Cal.	0.6200	1.7808
$\alpha_{max} = 30°$	Sim.	1.3890	3.8179
	Cal.	1.3869	3.9834

According to the results of the numerical simulation, the coefficients of Eq. (12) and Eq. (13) are estimated as follows:

k =7.0068e-04; k_1=1.9855; k_2=2.0654

c =0.0218; c_1=0.6941; c_2=1.7481

In Table 2 and Table 3, for f =1.5 and 2.5 Hz and a_{max}=10°, 20°, and 30°, the thrust force and the lateral force obtained by theoretical calculation and simulation are listed. The calculation results are in good agreement with the simulation results. Therefore, the thrust force and the lateral force are proportional to the exponent of the maximum swing angle and swing frequency.

In Fig. 11 (a), the red curves are the isothrust lines obtained according to Eq. (8). In Fig. 11 (b), the red curves are the isolateral force lines obtained according to Eq. (9). The thrust force curves and the lateral force curves obtained by multiple linear regression are consistent with simulation.

The variations in the instantaneous thrust force and instantaneous lateral force of undulatory fins with time are also studied with different maximum swing angles and different wave frequencies. Meanwhile, the results are fitted using polynomials and sine curves in order to explore whether the instantaneous thrust and lateral force meet similar undulating laws when the undulating fin is an approximate sine wave. The value of transient thrust changes with time in a period under different swing angles and frequencies is shown in Fig. 12. The value of the instantaneous lateral force with time in a period under different swing angles and frequencies is shown in Fig. 13. The amplitude of transient thrust force and transient lateral force fluctuation increases with increasing fin swing angle and wave frequency. The magnitude of the thrust force is always positive in the fluctuation period, and the change in the thrust force shows a periodic change of first decreasing and then increasing, then decreasing and then increasing. The direction of the transient lateral force will change during the swing of the undulatory fin. When passing through the middle position, the lateral force decreases to 0, and

Fig. 11 shows the contours of the thrust force F_{tm} and the lateral force F_{lm} produced by the various maximum swing angles against wave frequencies f at an inflow velocity U_0=0.01 m/s. The average thrust force and the average lateral force are assumed to be the exponent of the wave frequency and the maximum swing angle. The equations are as follows:

$$F_{tm} = k\alpha_{max}^{k_1} f^{k_2} \tag{8}$$

$$F_{lm} = c\alpha_{max}^{c_1} f^{c_2} \tag{9}$$

where k_1, k_2, c_1, and c_2 are exponents of the maximum swing angle and frequency, and k and c are scalecoefficients.

Taking the natural logarithm on both sides of Eq. (8) and Eq. (9), the formulation can be linearized:

$$\ln(F_{tm}) = \ln k + k_1 \ln(\alpha_{max}) + k_2 \ln f \tag{10}$$

$$\ln(F_{lm}) = \ln c + c_1 \ln(\alpha_{max}) + c_2 \ln f \tag{11}$$

To adopt the multivariate linear regression model, Eq. (10) and Eq. (11) are transformed into:

$$F_{tr} = k_r + k_1\alpha_r + k_2 f_r \tag{12}$$

$$F_{lr} = c_r + c_1\alpha_r + c_2 f_r \tag{13}$$

(a) *f*=1 Hz, $\alpha_{max} = 10°$

(b) *f*=1 Hz, $\alpha_{max} = 30°$

(c) *f* =2 Hz, $\alpha_{max} = 10°$

(d) *f*=2 Hz, $\alpha_{max} = 30°$

(e) *f* =3 Hz, $\alpha_{max} = 10°$
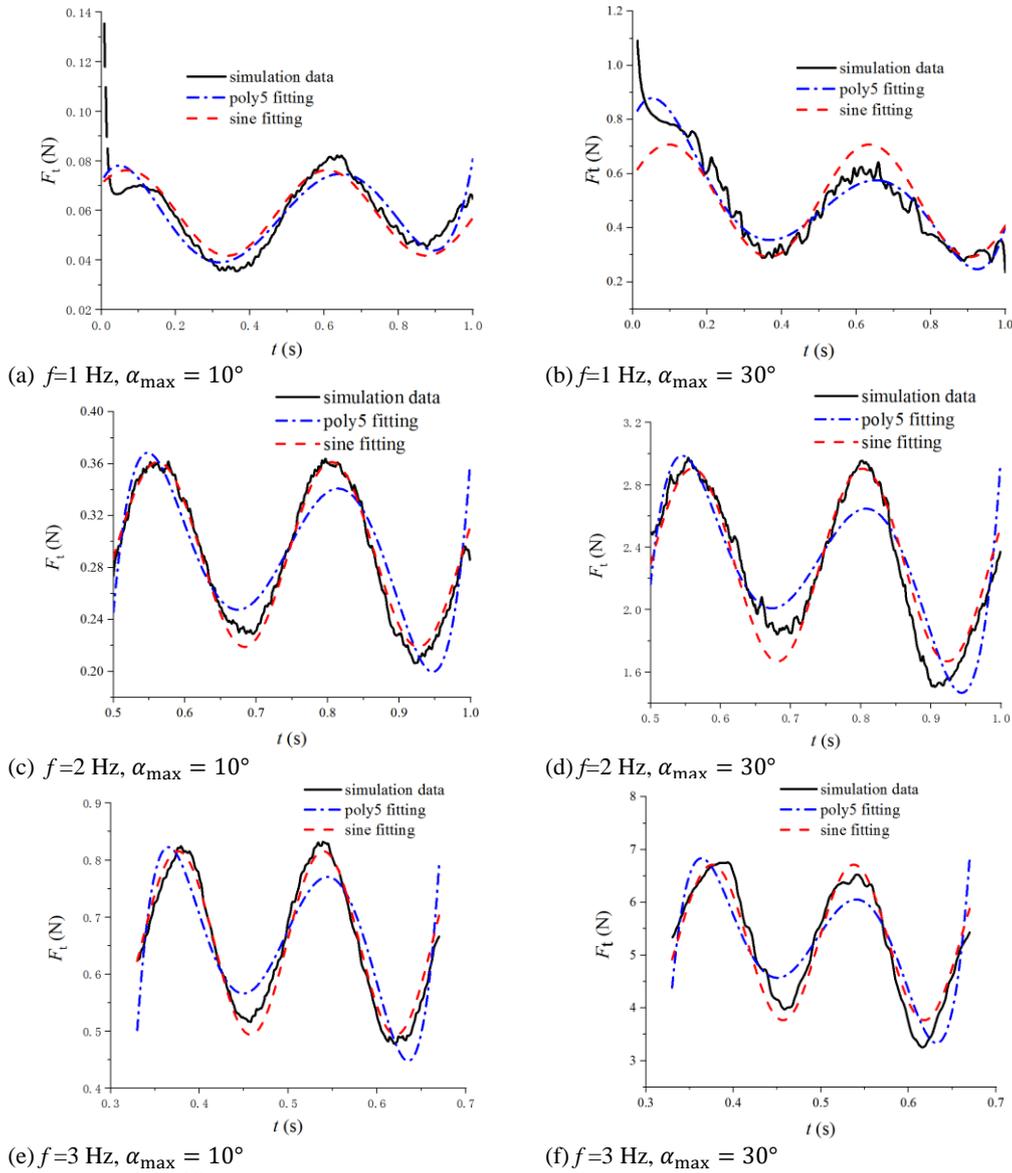
(f) *f* =3 Hz, $\alpha_{max} = 30°$

Fig. 12. Variation in thrust with time at different frequencies and swing angles.

the transient lateral force always fluctuates up and down near 0. To further study the variation in the transient thrust force and transient lateral force with time, a sine function (Eq. (14)) and quintic polynomial (Eq. (15)) are used to fit the simulation results. When the frequency is *f* =1 Hz, the transient thrust force varing with time is closer to a quintic polynomial. When the frequency is *f* =2 or 3 Hz, the change in transient thrust is closer to a sinusoidal change. However, regardless of how the fin swing angle and wave frequency change, the variation in the transient lateral force with time is closer to the quintic polynomial. The fitting curves of instantaneous thrust force and lateral force can be used for precise control and trajectory planning of the underwater vehicle with undulating fins. In addition, the internal relationship between instantaneous thrust and lateral force and fin wave shape can be used to optimize the shape of undulating fin.

$$F_t(t) = F_{t0} + A\sin\left[\pi(t-t_0)/\omega\right] \quad (14)$$

$$F_t(t) = a_0 + a_1 t + a_2 t^2 + a_3 t^3 + a_4 t^4 + a_5 t^5 \quad (15)$$

3.3. Effect of the Distance Between the Undulatory Fin and Bottom Surface on the Propulsion Performance

To study the influence of the distance between the undulatory fin and the bottom surface on the propulsion performance, the hydrodynamic characteristics of the undulatory fin under different maximum swing angles ($\alpha_{max} = 10°, 20°, 30°$), different wave frequencies (*f* = 1.0 Hz, 1.5 Hz, 2.0 Hz, 2.5 Hz, 3.0 Hz) and different distance ratios (*D*=0.2, 0.5, 1.0, 2.5, here *D*=*d*/*W*, *d* is the distance between the lower end of the undulatory fin and bottom surface) were investigated.

Fig. 14 shows the change in the surface pressure of the undulatory fin in a period when *D*=0.2, $\alpha_{max} = 30°$ and *f* = 2.5 Hz. Compared with the pressure distribution, without considering the influence of

(a) *f*=1 Hz, $\alpha_{max} = 10°$

(b) *f*=1 Hz, $\alpha_{max} = 30°$

(c) *f*=2 Hz, $\alpha_{max} = 10°$

(d) *f*=2 Hz, $\alpha_{max} = 30°$

(e) *f*=3 Hz, $\alpha_{max} = 10°$
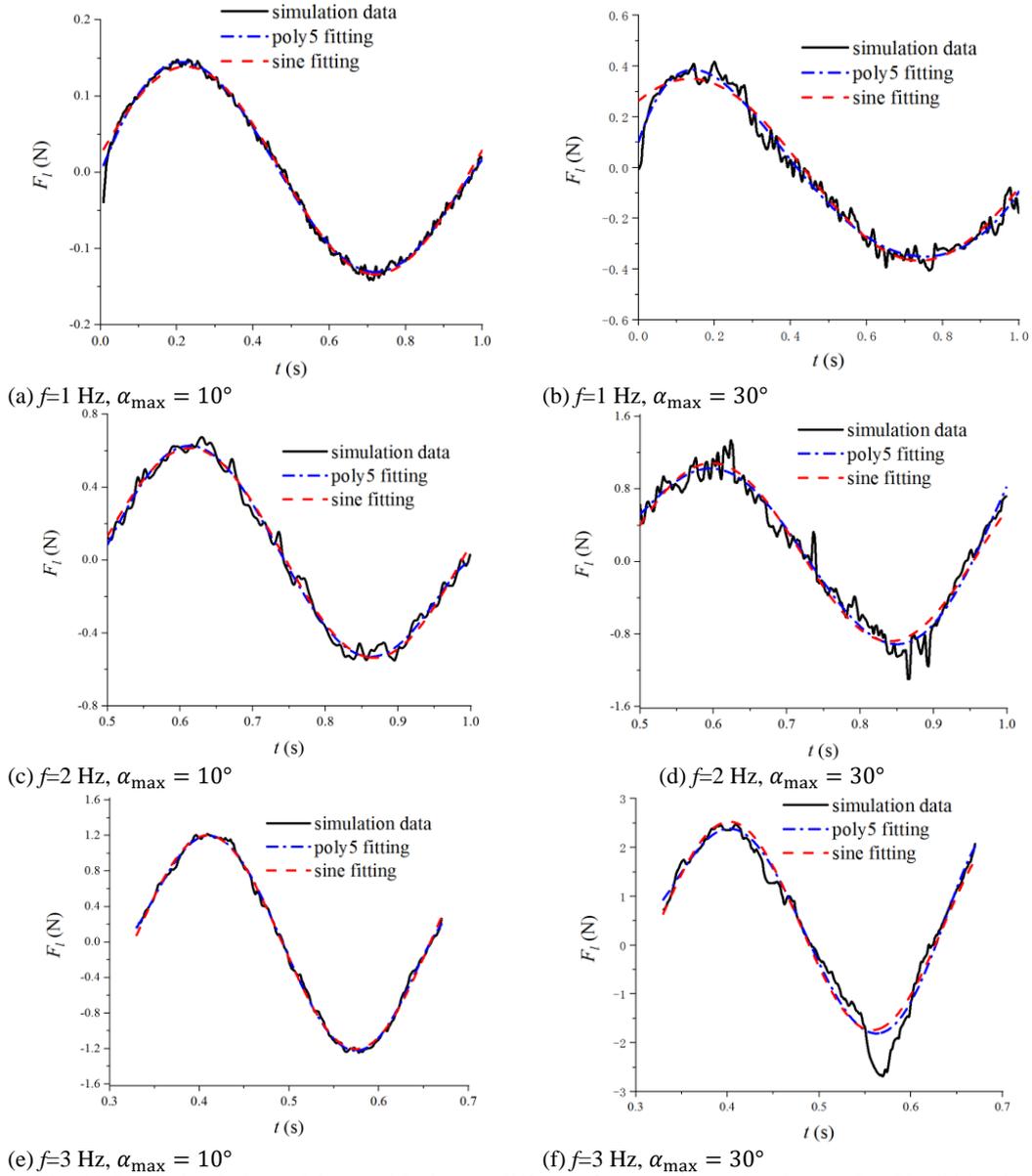
(f) *f*=3 Hz, $\alpha_{max} = 30°$

Fig. 13. Variation in lateral force with time at different frequencies and swing angles, U₀=0.01 m/s.

Fig. 14. Variation in pressure around the undulating fin (D = 0.2, $\alpha_{max} = 30°$, $f = 2.5$ Hz, U₀=0.01 m/s）.

(a) $\alpha_{max} = 10°$
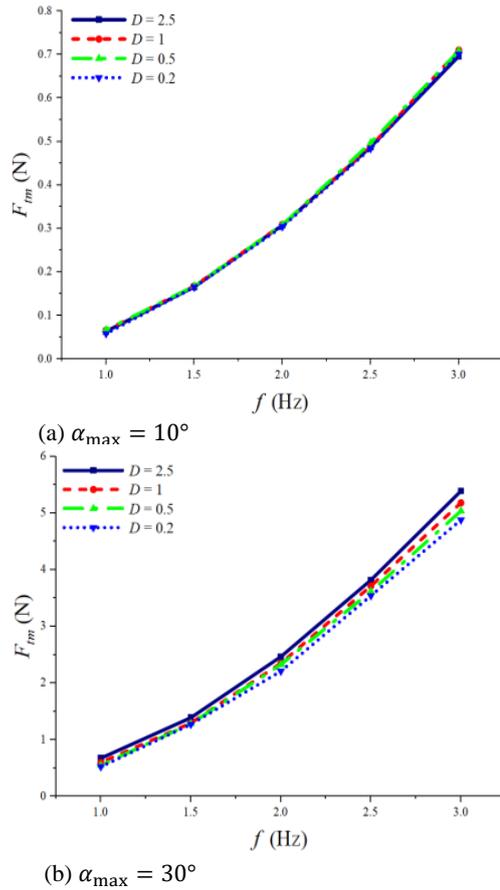

(b) $\alpha_{max} = 30°$

Fig. 15. Variation in thrust with frequency for undulating fins with different swing angles considering the distance from the underside, U_0=0.01 m/s.

(a) $\alpha_{max} = 10°$
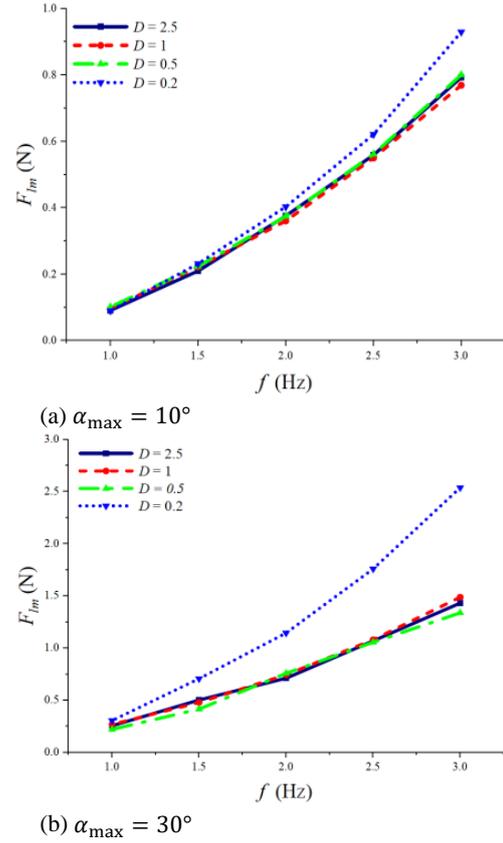

(b) $\alpha_{max} = 30°$

Fig. 16. Variation in lateral force with frequency for undulating fins with different swing angles considering the distance from the underside, U_0=0.01 m/s.

wall distance (Fig. 6), the fin surface pressure increases. In other words, the wall distance changes the thrust force and lateral force by affecting the pressure on the fin surface.

The average thrust force changes with fluctuation frequency in a period is shown in Fig. 15 when the distance ratio is D=0.2, 0.5, 1.0, and 2.5 and the maximum swing angles are $\alpha_{max} = 10°$ and 30°. The average thrust force decreases with decreasing distance ratio D when the fin swing angle is large and the swing frequency is high (such as $\alpha_{max} = 30°$ and $f = 3$ Hz). When the maximum angle $\alpha_{max} = 10°$, the average thrust hardly changes with the change in the distance between the fluctuating fin and the bottom surface. The thrust force of the undulatory fin is hardly affected by the distance between the undulatory fin and the bottom surface, and it has good propulsion performance even when working close to the underwater bottom surface.

Figure 16 shows the variation in the average lateral force with fluctuation frequency in a period when the distance ratio D=0.2, 0.5, 1.0, and 2.5 and the maximum swing angles $\alpha_{max} = 10°$ and 30°. When the distance ratio is D=0.5, 1.0, and 2.5, the value of the lateral force is almost constant, and when D=0.2, the lateral force increases

significantly. We know that the lateral force is related to the energy consumption of the undulating fin, so when the distance ratio D=0.2, the power consumption will increase (Chen *et al.* 2020).

Taking the average thrust force value of distance ratios D=2.5 as a reference F_{tr}, the nondimensional average thrust force of different distance ratios changing with wave frequency is shown in Fig. 17.

When the maximum swing angles is at $\alpha_{max} = 10°$, the nondimensional average thrust force reaches the maximum value at distance ratios D=0.5. When the distance ratio D=0.2 and D=2.5, their dimensionless average thrust force is approximately equal. When the maximum swing angles is at $\alpha_{max} = 30°$, the nondimensional average thrust force discreases with discreasing distance ratio. The larger the fluctuation frequency is, the greater the amplitude of thrust decreases.

Taking the average lateral force value of distance ratios D=2.5 as a reference F_{lr}, the nondimensional average lateral force of different distance ratios changing with wave frequency is shown in Fig. 18. When the maximum swing angles $\alpha_{max} = 10°$, the nondimensional average lateral force reaches the minimum value at distance ratios D=1.0. When the maximum swing angles $\alpha_{max} = 30°$, the nondimensional average lateral force reaches the minimum value at distance ratios D=0.5.

(a) $\alpha_{\max} = 10°$

(a) $\alpha_{\max} = 10°$
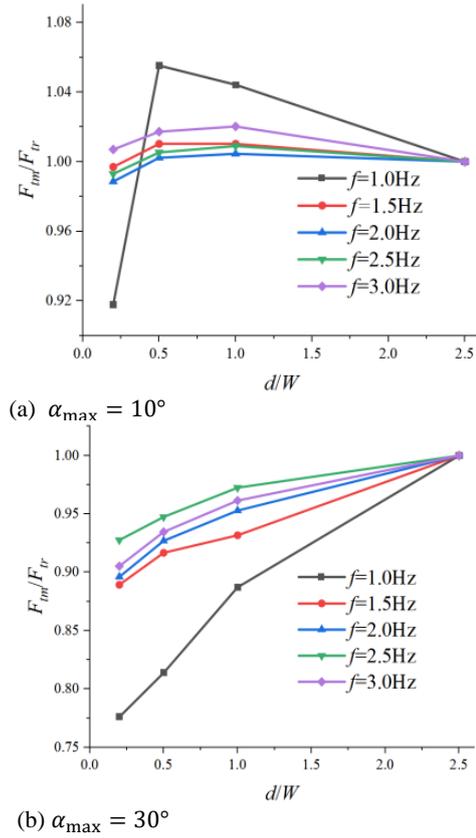

(b) $\alpha_{\max} = 30°$

(b) $\alpha_{\max} = 30°$

Fig. 17. Variation in thrust with frequency for undulating fins with different swing angles considering the distance from the underside, U₀=0.01 m/s.
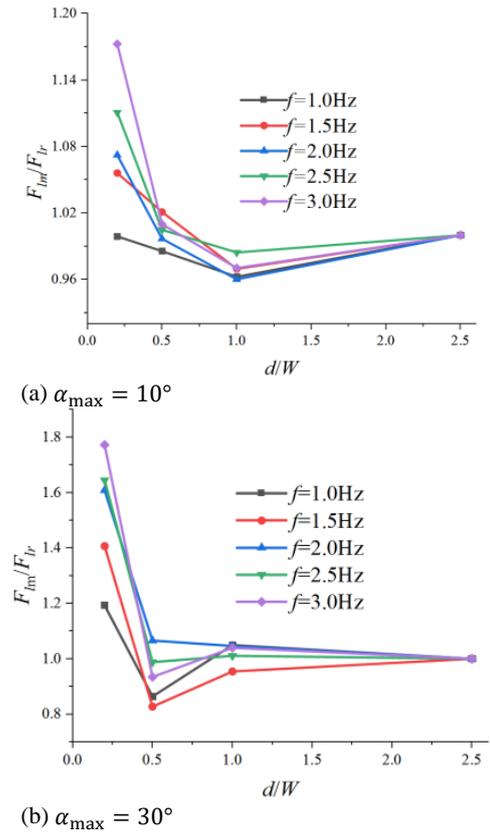
Fig. 18. Variation in lateral force with frequency for undulating fins with different swing angles considering the distance from the underside, U₀=0.01 m/s.

Figure 19 shows the distribution of streamlines around the fluctuating fin at different times when the distance ratio is *D*=0.2 and 2.5, the maximum swing angle of the fin is $\alpha_{\max} = 30°$, and the fluctuating frequency *f* = 2.5 Hz. When the distance ratio between the undulary fin and the bottom is *D*=2.5, two groups of large vortices are generated at the tail and lower edge of the undulatory fin, which

are shown in Fig. 19 (a) and Fig. 19 (c). The streamline distribution of the distance ratio *D*=0.2 is shown in Fig. 19 (b) and 19 (d) when the time is at *t*=0 s and *t*=0.3 s. No obvious vortex is formed due to the small distance between the undulatory fin and the bottom surface. However, part of the lateral vortex is transferred from the lower end to the
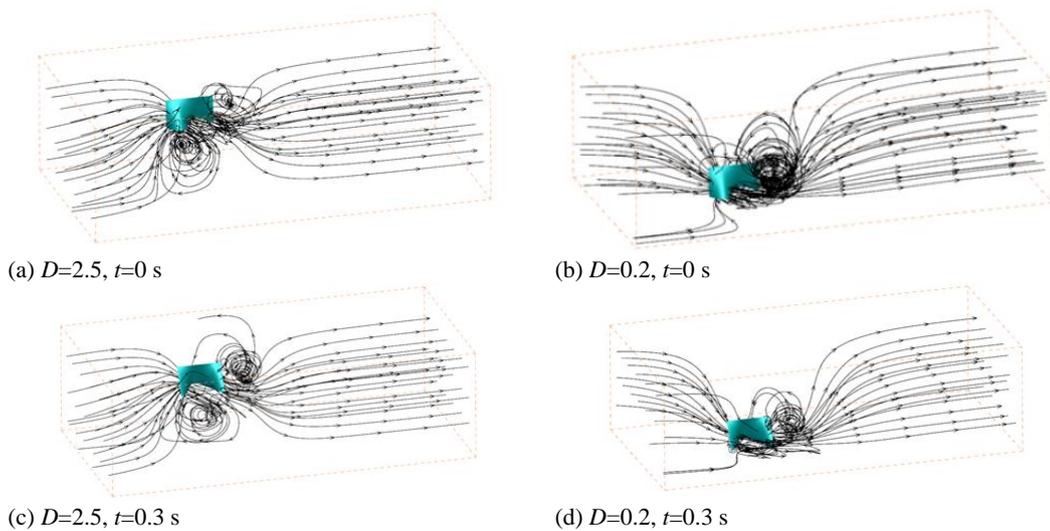

(a) *D*=2.5, *t*=0 s

(b) *D*=0.2, *t*=0 s

(c) *D*=2.5, *t*=0.3 s

(d) *D*=0.2, *t*=0.3 s

Fig. 19. Distribution of streamlines around undulating fins, *a*max=30°, *f* = 2.5 Hz, U₀=0.01 m/s.

trailing edge of the undulatory fin, which combines with the tail vortex. So the jet generated by the shedding of the Karman vortex street forms an included angle with the moving direction of the undulating fin, thus reducing the thrust in the moving direction of the undulating fin. Because the main thrust of the undulating fin comes from the pressure difference of the fin surface, the total thrust of undulating fin decreased slightly.

On the other hand, part of the vortex is transferred to the two sides of the undulatory fin to form dense vortices on the sides of the undulatory fin, which increases the lateral force of the undulatory fin.

4. CONCLUSIONS

In this paper, an undulatory fin propeller is designed taking the electric eel as the bionic object. The Hydrodynamic characteristics of undulating fins and the influence of maximum swing angle, wave frequency and wall effect are studied.

(1) The average thrust and lateral force change exponentially with the maximum swing angle and fluctuation frequency. The high-pressure area is at the front edge of the concave surface of the undulatory fin. There are opposite rotation vortices generated at the leading edge of the undulatory fin, gradually spread and finally fall off at the trailing edge.

(2) The transient thrust force and lateral force fluctuate approximately sine with time. When the swing angle increases, their maximum fluctuation amplitude increases. The instantaneous thrust is always positive, and the instantaneous lateral force fluctuates up and down around the zero point. In a motion period, the number of fluctuations of lateral force is approximately 1/2 of that of thrust force. When the frequency f=1 Hz, the variation in the transient thrust force with time is closer to the quintic polynomial. When the frequency is f=2 or 3 Hz, the change in transient thrust is closer to a sinusoidal change. However, regardless of how the fin swing angle and wave frequency change, the change of the transient lateral force with time is more approximate to quintic polynomial.

(3) The average thrust of the undulatory fin decreases with decreasing distance ratio D, but the decrease range is small. Especially when the fin is at the maximum swing angle $\alpha_{max} = 10°$, the propulsion performance can be maintained with discreasing the distance between the fluctuating fin and the bottom surface. When the distance ratio is D=0.2 and the maximum swing angle $\alpha_{max} = 30°$, the lateral force is greatly higher than that of other situations. Namely, the power consumption of the undulatory fin will increase with decreasing distance ratio.

(4) When the maximum swing angles $\alpha_{max} = 10°$, the nondimensional average thrust force reaches the maximum value at distance ratios D=0.5. The nondimensional average lateral force reaches the minimum value at distance ratios D=1.0. When the maximum swing angles $\alpha_{max} = 30°$, the

nondimensional average thrust force discreases when the fin is close to the wall. The nondimensional average lateral force reaches the minimum value at distance ratios D=0.5.

(5) When the undulatory fin is close to the bottom surface, part of the vortex around the lower edge is transferred to the trailing edge of the undulatory fin, which combines with the tail vortex to prevent the normal shedding of the tail vortex, resulting in the reduction of the thrust of the undulatory fin. The other part of the vortex is transferred to the two sides of the undulatory fin, forming a dense vortex on the side of the undulatory fin and causing the lateral force of the undulatory fin to increase.

DATA AVAILABILITY STATEMENT

The data that support the findings of this study are available from the corresponding author upon reasonable request.

CONFLICTS OF INTEREST

The author(s) declare no potential conflicts of interest with respect to the research, authorship, and/or publication of this article.

FUNDING STATEMENT

REFERENCES

Alqahtani, S., H. M. Ali, F. Farukh and K. Kandan (2023). Experimental and computational analysis of polymeric lattice structure for efficient building materials. *Applied Thermal Engineering* 218(5), 119366.

Arslan, E. and A. Kadir (2019). A design methodology for cuttlefish shaped amphibious robot. *Avrupa Bilim ve Teknoloji Dergisi* 214-224.

Chen, H., D. Zhao and Y. Wang (2020). Simulation of flow field of the undulate propulsion for biomimetic stingray ring pectoral fins. *Computer Simulation* 37(3), 333-338.

Deng, Y. (2015). *Study on Key Technologies of New Water-Jet-Propulsion Type Underwater Robot.* M. S. thesis, Beijing Institute of Technology, Beijing, China.

Hussain, I., F. Bibi, S. A. Bhat, U. Sajjad, M. Sultan, H. M. Ali, M. W. Azam, S. K. Kaushal, S. Hussain and W. Yan (2022). Evaluating the parameters affecting the direct and indirect evaporative cooling systems. *Engineering Analysis with Boundary Elements* 145, 211-223.

He, J. H., Y. H. Zhang and K. H. Low (2015). Comparative study of effect of fin arrangement on propulsion performance of bio-inspired underwater vehicles with multiple SMA fins. *International Journal of Advanced Robotic Systems* 12(9), 135.

Kato, N. (2005). Median and paired fin controllers for biomimetic marine vehicles. *Transactions of the ASME* 58, 238-252.

Lawag, R. A. and H. M. Ali (2022). Phase change materials for thermal management and energy storage: A review. *Journal of Energy Storage* 55, Part C, 105602.

Li, Q., J. Zhang, J. Hong, D. Hu, Y. Yang and S. Guo (2021). A novel undulatory propulsion strategy for underwater robots. *Journal of Bionic Engineering* 18(4), 812-823.

Liu, F. (2015). *Research on Propulsion Performances of Flexible Undulating Fin Based Biomimetic System*. Ph. D. thesis, Zhejiang University. Zhejiang, China.

Liu, H. and O. Curet (2018). Swimming performance of a bio-inspired robotic vessel with undulating fin propulsion. *Bioinspiration & biomimetics* 13(5), 056006.

Liu, L., Y. Li, Y. Wang and X. Ma (2020). Design and preliminary evaluation of a biomimetic underwater robot with undulating fin propulsion. *In IOP Conference Series: Materials Science and Engineering*, IOP Publishing.

Luo, Y., Q. Xiao, G. Shi, L. Wen, D. Chen and G. Pan (2020). A fluid–structure interaction solver for the study on a passively deformed fish fin with non-uniformly distributed stiffness. *Fluids and Structures* 92, 102778.

Ma, R., Y. Wang, R. Wang, and S. Wang (2019). Development of a propeller with undulating fins and its characteristics. *In 2019 IEEE International Conference on Real-time Computing and Robotics (RCAR)*, IEEE.

Mivehchi, A., J. Dahl and S. Licht (2016). Heaving and pitching oscillating foil propulsion in ground effect. *Fluids and Structures* 63, 174-187.

Moored, K. W. (2018). Unsteady three-dimensional boundary element method for self-propelled bio-inspired locomotion. *Computers & Fluids* 167, 324-340.

Mohamad, O., G. Mehdi, R Lotfi and R. Muhammad (2022). Performance analysis of bio-inspired transformable robotic fish tail. *Ocean Engineering* 244, 110406.

Nguyen, V. D., C. A. T. Pham, V. H. Nguyen, T. P. Tran and T. T. Nguyen (2018). Modular design of gymnotiform undulating fin. *In International Conference on Advanced Engineering Theory and Applications*, Springer, Cham.

Pang, S., F. Qin, W. Shang, S. Cong and S. Zhang (2021). Optimized design and investigation about propulsion of bionic Tandem undulating fins I: Effect of phase difference. *Ocean Engineering* 239, 109842.

Park, S. G., B. Kim and H. J. Sung (2017). Hydrodynamics of a self-propelled flexible fin near the ground. *Physics of Fluids* 29(5), 051902.

Shi, G. and Q. Xiao (2021a). Numerical investigation of a bio-inspired underwater robot with skeleton-reinforced undulating fins. *European Journal of Mechanics-B/Fluids* 87, 75-91.

Shi, G., Q. Xiao and E. Boulougouris (2021b). Ground effects on the propulsion of an undulating pectoral fin with various aspect ratios. *Journal of Fluids and Structures* 106, 103388.

Sun, X., J. Zhang, H. Li, and D. Huang (2019). Parametric study of an undulating plate in a power-extraction regime. *Mechanical Science and Technology* 33(1), 255-268.

Suzuki, H. and N. Kato (2005). A numerical study on unsteady flow around a mechanical pectoral fin. *International Journal of Offshore and Polar Engineering* 15(3), 161-167.

Wang, Y., J. Tan and D. Zhao (2015). Design and experiment on a biomimetic robotic fish inspired by freshwater stingray. *Bionic Engineering* 12(2), 204-216.

Wang, Y., R. Wang, S. Wang, M. Tan, and J. Yu (2019). Underwater bioinspired propulsion: From inspection to manipulation. *IEEE Transactions on Industrial Electronics* 67(9), 7629-7638.

Wei, C., Q. Hu, Y. Liu, S. Yin, Z. Chen and X. Ji (2021). Performance evaluation and optimization for two-dimensional fish-like propulsion. *Ocean Engineering* 233, 109191.

Xiao, J. K., Y. X. Huang, Z. W. Lin and M. W. Huang (2021). Design of Amphibious Robot Based on the Motion Mode of Electric Eels. *Mechanical Research & Application* 34 (1), 89-92.

Yin, S., Q. Hu, Y. Zeng, C. Wei and Z. Chen (2021). Kinetic analysis and design of a bio-inspired amphibious robot with two undulatory fins. *In 2021 IEEE International Conference on Real-time Computing and Robotics (RCAR)*, IEEE.

Zawawi, N. N. M., W. H. Azmi, M. F. Ghazali and H. M. Ali (2022). Performance of air-conditioning system with different nanoparticle composition ratio of hybrid nanolubricant. *Micromachines* 13(11), 1871.

Zhang, C., H. Huang and X. Y. Lu (2017). Free locomotion of a flexible plate near the ground. *Physics of Fluids* 29(4), 041903.

Zhang, T., R. Wang, Y. Wang, L. Cheng, S. Wang and M. Tan (2021). Design and locomotion control of a Dactylopteridae-inspired biomimetic underwater vehicle with hybrid propulsion. In *IEEE Transactions on Automation Science and Engineering*, IEEE.

Zhang, J., Y. Bai, S. Zhai and D. Gao (2019). Numerical study on vortex structure of undulating fins in stationary water. *Ocean Engineering* 187, 106166.

Zhao, Z. and L. Dou (2019). Computational research on a combined undulating-motion pattern considering undulations of both the ribbon fin and fish body. *Ocean Engineering* 183, 1-10.

Zhou, H., T. Hu, H. Xie, D. Zhang and L. Shen (2010). Computational hydrodynamics and statistical modeling on biologically inspired undulating robotic fins: a two-dimensional study. *Bionic Engineering* 7(1), 66-76.